AERODYNAMICS AND AEROACOUSTICS OF SUBSONIC AND TRANSONIC ROTORS IN HOVER AND FORWARD FLIGHT

M. Gennaretti,* U. Iemma,† F. Salvatore‡ and L. Morino§
Dipartimento di Ingegneria Meccanica e Industriale
Università Roma Tre, via C. Segre 60, 00146 Rome, Italy
E-mail: massimo@seine.dma.uniroma3.it

Abstract

Some recent developments in aerodynamic and aeroacoustic analysis of wings and rotors by using a boundary integral methodology for potential flows are presented. The analysis covers subsonic and transonic full–potential flows around wings and hovering and forward–flight rotors. A coupled viscous/inviscid technique is utilized to take into account the effects of the viscosity, in the limited case of steady attached high–Reynolds number flows. The emphasis is on the numerical applications (specifically on the effects of the unsteadiness, of the viscosity, and of the transonic nonlinearities) but the theoretical formulation is briefly addressed. Comparisons of numerical results are included.

Introduction

The scope of this work is to present an overview of some recent developments in the aerodynamic and aeroacoustic analysis of lifting bodies in arbitrary motion, based on a boundary integral methodology for the velocity potential, introduced by Morino [1]. For unsteady subsonic flows, the solution for the velocity potential is given by a direct boundary integral representation extended over the surfaces of the body and of the wake. For transonic flows, the integral representation for the velocity potential includes also a field integral extended over the portion of the fluid field where nonlinear terms are not negligible (*e.g.*, blade tips for helicopter rotors). The inclusion of the effects of viscosity is obtained by a viscous/inviscid coupling technique.

A detailed review of the field is beyond the scope of this paper. Extensive reviews of the present methodology are given in [2] and [3], where the emphasis is on the theoretical aspects of the boundary integral formulation for potential flows and its extension to viscous flows. Here, the emphasis is on the numerical validation, in particular on the analysis of the effects of the viscosity and of the transonic nonlinearities. Numerical results include applications to subsonic and transonic potential flows, and transonic high–Reynolds viscous flows. The methodology used for the analysis of subsonic flows around fixed wings and rotors is that presented in Gennaretti [4] where a unified aerodynamic/aeroacoustic methodology is proposed. The extension to the analysis of transonic flows is based on the full–potential formulation presented in Iemma [5]. Finally, for attached high–Reynolds number flows, the effects of the viscosity are included by using a viscous/inviscid coupling technique as discussed by Salvatore [6].

The present paper is an update of Refs. [7] and [8]. Specifically, it differs from Ref. [7] in that results for aeroacoustics of rotors in hover and in forward flight in subsonic and transonic flow have been included, and contains an update of the results for viscous flows given in [8]. Also, the results presented in this paper were partially obtained under a BRITE-EURAM project, HELISHAPE, which is reported in full in Ref. [9].

Theoretical Formulation

As stated in the Introduction, the emphasis in this paper is on the numerical applications of the present methodology. However, for the sake of completeness, the theoretical formulation is briefly outlined in this section. First, the potential formulation for the study of inviscid flows is addressed; then, the boundary integral representation used for the solution of the equation of the velocity potential is presented; finally,

* Assistant Professor
† Assistant Professor
‡ Research Scientist
§ Full Professor, AIAA Member

the boundary–layer/full–potential coupling technique is described.

Full–Potential Flow Formulation

An isentropic, initially irrotational flow of an inviscid, non-conducting fluid remains isentropic and irrotational at all times. Under these assumptions the velocity field may be expressed in terms of a scalar potential φ such that $\mathbf{v} = \nabla\varphi$, where $\mathbf{v}$ is the fluid velocity. Combining the continuity equation, written in conservative form, and Bernoulli's theorem, one obtains the following equation for the velocity potential

$$\nabla^2\varphi - \frac{1}{a_\infty^2}\frac{\partial^2\varphi}{\partial t^2} = \sigma, \qquad (1)$$

where $a_\infty^2 = \gamma\, p_\infty/\rho_\infty$ is the speed of sound in the undisturbed flow, whereas σ denotes all the nonlinear terms, given by (see, *e.g.*, [10])

$$\sigma = \nabla\cdot\left[\left(1-\frac{\rho}{\rho_\infty}\right)\nabla\varphi\right] - \frac{\partial}{\partial t}\left(\frac{\rho}{\rho_\infty} + \frac{1}{a_\infty^2}\frac{\partial\varphi}{\partial t}\right) \qquad (2)$$

Hence, the velocity potential is governed by a nonlinear wave equation (with ρ obtained from the Bernoulli theorem).
The boundary and initial conditions for Eq. 2 are obtained as follows. The surface of the body, $\mathcal{S}_B$, is assumed to be impermeable. This yields

$$\frac{\partial\varphi}{\partial n} = \mathbf{v}_B \qquad (\mathbf{x} \in \mathcal{S}_B), \qquad (3)$$

where $\mathbf{v}_B$ denotes the velocity of a point $\mathbf{x} \in \mathcal{S}_B$. Furthermore, in a frame of reference fixed with the unperturbed fluid, we have $\varphi = 0$ at infinity. In the potential–flow formulation, the wake is a surface of discontinuity for the velocity potential, hence boundary conditions over the wake and at the trailing edge are also required (see [2] and [3], for details). Using the principles of conservation of mass and momentum across the wake surface, $\mathcal{S}_W$, one obtains that the prerssure is continuous across $\mathcal{S}_W$ and that $\mathcal{S}_W$ is impermeable (*i.e.*, $\mathbf{v}\cdot\mathbf{n} = \mathbf{v}_W\cdot\mathbf{n}$, where the velocity of a point on $\mathcal{S}_W$, $\mathbf{v}_W$, is defined as the average of the velocity of the fluid on the two sides of the wake). In terms of the velocity potential, the first condition yields $\Delta(\partial\varphi/\partial n) = 0$, whereas the second one, using Bernoulli's theorem, yields

$$\frac{D_W}{Dt}(\Delta\varphi) = 0, \qquad (4)$$

where $D_W(\,)/Dt := \partial(\,)/\partial t + \mathbf{v}_W\cdot\nabla(\,)$. This condition implies that the value of $\Delta\varphi$ remains constant in time following a wake point $\mathbf{x}_W$ (having velocity $\mathbf{v}_W$) and equals the value it had when $\mathbf{x}_W$ left the trailing edge. This value is obtained by imposing the trailing-edge condition that, at *the trailing edge points, $\Delta\varphi$ on the wake equals* $\Delta\varphi = \varphi_u - \varphi_l$ on the body (subscripts u and l denote, respectively, upper and lower sides of the body surface).
Finally, we assume homogeneous initial conditions.

Boundary Integral Formulation

In order to address the boundary integral formulation for the solution of the nonlinear wave equation 1, let us consider two disjoint closed rigid surfaces $\mathcal{S}_B$ and $\mathcal{S}_W$ surrounding, respectively, the volume $\mathcal{D}_B$ occupied by the body and the volume $\mathcal{D}_W$ occupied by a thin fluid region containing the wake surface, which is assumed to be undeformed (see later). It may be shown that the integral representation for the wave equation, Eq. 1, is given by (*see [2] for details*)

$$E(\mathbf{x},t)\varphi(\mathbf{x},t) = \mathcal{I}_B + \mathcal{I}_W + \iiint_{\mathcal{V}}[G_0\,\sigma]_{t=t_*-\theta}\,d\mathcal{V}, \qquad (5)$$

where $E(\mathbf{x},t) = 1$ if $\mathbf{x} \in \mathcal{V}$ (with $\mathcal{V}$ denoting the fluid region where the nonlinear terms are not negligible) and $E(\mathbf{x},t) = 0$ otherwise; in addition, θ is the propagation time from $\mathbf{y}$ to $\mathbf{x}$, and $G_0 = -1/4\pi\|\mathbf{r}\|\,|1-M_r|$ (where M_r is the component of the Mach vector in the direction $\mathbf{r} = \mathbf{x}-\mathbf{y}$).
Finally, $\mathcal{I}_B$ and $\mathcal{I}_W$ are given by an expression of the type

$$\begin{aligned}\mathcal{I}(\mathbf{x},t) = &\iint_{\mathcal{S}}\left[\frac{\partial\varphi}{\partial\tilde{n}}G_0 - \varphi\frac{\partial G_0}{\partial\tilde{n}}\right]_{t=t_*-\theta}d\mathcal{S} \qquad (6)\\ &+\iint_{\mathcal{S}}\left[G_0\frac{\partial\varphi}{\partial t}\left(\frac{\partial\theta}{\partial\tilde{n}} + 2\frac{\mathbf{v}_x\cdot\mathbf{n}}{a_\infty^2}\right)\right]_{t=t_*-\theta}d\mathcal{S}\\ &+\frac{1}{a_\infty^2}\iint_{\mathcal{S}}\left[\varphi G_0\frac{\partial}{\partial t}[\mathbf{v}_x\cdot\mathbf{n}(1-\mathbf{v}_x\cdot\nabla\theta)]\right]_{t=t_*-\theta}d\mathcal{S},\end{aligned}$$

with $\mathcal{S} = \mathcal{S}_B$ for $\mathcal{I}_B$, and $\mathcal{S} = \mathcal{S}_W$ for $\mathcal{I}_W$. In Eq. 6, $\partial(\,)/\partial\tilde{n} := \partial(\,)/\partial n - \mathbf{v}_x\cdot\mathbf{n}\;\mathbf{v}_x\cdot\nabla(\,)/a_\infty^2$, whereas $\mathbf{v}_x$ represents the velocity of a point $\mathbf{x}$ (of the space connected with the surface $\mathcal{S}$) with respect to the air space.
Equation 5, with $\mathcal{I}_B$ and $\mathcal{I}_W$ given by Eq. 6, is the boundary integral representation for the solution to Eq. 1 with initial and boundary conditions as

specified above. Note that, for the contribution $\mathcal{I}_W$ of the wake surface $\mathcal{S}_W$, using $\Delta(\partial\varphi/\partial n) = 0$ yields that the integral depends upon $\Delta\varphi$ only. Hence, Eq. 5 may be used to evaluate the potential φ at $\mathbf{x}$, if φ and $\partial\varphi/\partial n$ are known on $\mathcal{S}_B$, $\Delta\varphi$ on $\mathcal{S}_W$, and σ in $\mathcal{V}$.

In the absence of the wake and for linear flows (*i.e.*, with σ neglected) $\mathcal{I}_W$ and the volume integral in Eq. 5 disappear. Thus, if $\mathbf{x}$ tends to the boundary, Eq. 5 yields a compatibility condition between φ and $\partial\varphi/\partial n$ on $\mathcal{S}_B$, which must be satisfied by the solution of the problem. In our case $\partial\varphi/\partial n$ on $\mathcal{S}_B$ is known from the boundary condition on $\mathcal{S}_B$, Eq. 3. Hence, such a compatibility condition is an integral equation for φ on the boundary $\mathcal{S}_B$. Next, consider the lifting case, for which the presence of the wake is necessary (cfr. the d'Alembert paradox, see [2] and [3]). To include the wake contribution, two different approaches are used. For fixed wings and hovering rotors, we express the wake contribution in a frame of reference fixed with the body and hence the wake integral is still given by Eq. 6 (with the last integral vanishing). For rotors in forward flight, we assume that the wake deformation is negligible (*i.e.*, the wake is the surface swept by the trailing edge, as we have assumed for the results presented here). Thus, the wake contribution is expressed in the air frame. In either case, if the wake geometry is prescribed, the solution is obtained using an approach similar to that used for nonlifting problems with $\Delta(\partial\varphi/\partial n) = 0$, and $\Delta\varphi$ given by Eq. 4.

Finally, for transonic flows, one has to consider also the nonlinear contribution of the volume integral in Eq. 5; this is obtained by iteration where σ is evaluated step by step from the computed values of φ in the field (see [5] for details). Note that, in general, the geometry of the wake is unknown and is part itself of the solution (free–wake analysis). Here, we do not present free–wake results and, for the sake of conciseness, the reader is referred to [2] and [3] for details.

Once φ on the surface is known, φ and hence $\mathbf{v}$ may be evaluated anywhere in the field. Then the pressure (and hence, the acoustic noise) may be computed using the Bernoulli theorem. Note that, this approach is considerably different from the classical aeroacoustic formulations based either on the Ffowcs Williams and Hawkings equation or the Kirchhoff surface.

Viscous/Inviscid Coupling

In this subsection, the viscous/inviscid coupling technique that has been used to include the effects of viscosity in the potential model presented above is described. Specifically, a classical coupling technique has been adapted to the specific boundary integral formulation used here for the solution of the inviscid flow.[1]

The present analysis is limited to the case of attached steady two–dimensional high–Reynolds number flows, where it is assumed that the viscous vortical region (*i.e.*, boundary layer and wake) has a small thickness, δ. Under these assumptions, a classical boundary–layer formulation may be used. Outside the boundary layer and wake, the flow is irrotational and is solved by using a full–potential model obtained by introducing, in the boundary integral formulation described above, a viscous–flow correction based on Lighthill's equivalent sources approach [11] (see also [12], for a recent developments in this field). The matching of the boundary–layer solution with the potential–flow solution with viscosity correction is obtained through iteration.

Specifically, the boundary–layer equations are solved in integral form; for attached flows, this approach yields comparably accurate predictions at considerably reduced computational costs in comparison with differential methods. The laminar portion of the boundary layer is computed by combining Thwaites' collocation method for incompressible flows [13], with the Illingworth-Stewartson coordinate transformation (see, *e.g.*, [14]) to take into account compressibility effects. The transition from laminar to turbulent flow is detected by the semi–empirical Michel's method [15]. The turbulent portion of the boundary layer and the wake are studied by the 'lag-entrainment' method of Green, Weeks and Brooman [16], according to which, the classical von Kármán boundary–layer equation is combined with an equation taking into account the flow entering the boundary-layer (entrainment equation), and an equation for the evolution of the turbulent kinetic energy (lag equation). Finally, classical semi–empirical algebraic relationships are utilized which complete the formulation of the problem (see Salvatore [6], for details).

[1] The present coupling technique is described here in some details since it is not addressed in [2] (where the formulation is limited to potential flows) and is barely touched upon in [3].

Once the boundary–layer equations are solved, the viscous–flow correction for the potential–flow model may be evaluated. Such correction is given in terms of a transpiration flow across $\mathcal{S}_B$ and $\mathcal{S}_W$ which, according to Lighthill [11], takes into account the displacement of the potential–flow streamlines due to the presence of the vortical layer around the body and wake surfaces. The intensity of the compressible–flow transpiration velocity is given by (see, *e.g.*, Lemmerman and Sonnad [17])

$$\sigma_V = \frac{1}{\rho_e u_e}\left[\frac{\partial}{\partial s_1}(\rho_e u_e \delta_1^*) + \frac{\partial}{\partial s_2}(\rho_e u_e \delta_2^*)\right], \quad (7)$$

where s_i $(i = 1, 2)$ denote orthogonal arclengths over the surface of the body, δ_i^* are displacement thicknesses in directions s_i, whereas u_e and ρ_e denote, respectively, the magnitude of velocity (in a reference fixed with the body) and the density, both at the outer edge of the vortical layer. As a consequence, the boundary condition for φ over the body surface is modified as follows (cfr. Eq. 3):

$$\frac{\partial \varphi}{\partial n} = \mathbf{v}_B \cdot \mathbf{n} + \sigma_V \qquad (\mathbf{x} \in \mathcal{S}_B), \quad (8)$$

whereas, on the wake surface $\mathcal{S}_W$, one has

$$\Delta\left(\frac{\partial \varphi}{\partial n}\right) = (\sigma_V)_u + (\sigma_V)_l \qquad (\mathbf{x} \in \mathcal{S}_W), \quad (9)$$

where the subscripts u and l refer to quantities evaluated, respectively, in the vortical layers on the upper and lower sides of $\mathcal{S}_W$.
Thus, the solution of the potential–flow equations containing the viscous correction above gives a prediction for u_e, ρ_e, and M_e (the subscript e denotes evaluation at the outer edge of the boundary layer) which are in turn the input for the boundary–layer solution and hence for the evaluation of σ_V (direct method). For separated flows (not examined here), the set of differential equations for the boundary layer is singular and an iterative technique based on the inverse solution method is typically employed; however, this type of analysis is beyond the scope of the present work, which is limited to attached–flow analysis (*e.g.*, wings at small angles of attack, absence of strong shocks).

Numerical Results

The formulation presented above has been applied in the past to the numerical analysis of the aerodynamics of wings as well as rotors in several flight conditions. As stated in the Introduction, here we present some numerical results recently obtained so as to give an overall picture of the level of development and validation achieved thus far. For inviscid flows, the cases under examination cover rotors in subsonic forward flight and transonic analysis of wings and rotors in hover and forward flight, including the aeroacoustic analysis. In addition, results for the viscous/inviscid interaction in the limited case of steady two–dimensional attached high–Reynolds number viscous flows in the transonic range are presented.

Potential Subsonic Advancing Rotors

For the analysis of potential subsonic hovering rotors, we present some numerical results obtained by studying the configuration considered in [18] at the DNW for the experimental program within the HELINOISE project. The rotor tested in this program is a 40% geometrically and dynamically scaled model of a four–bladed, hingless BO-105 main rotor. The rotor has a diameter of 4m with a root cut-out of 0.35m and a chord length of 0.121m. The blades have a $-8°$ of linear twist, with a modified NACA 23012 profile, and a coning angle of 2.5°. The nominal rotor operational speed is 1040rpm. In the present analysis the rotor is in ascent flight, with an effective tip path plane angle $\alpha'_{TPP} = -14.63°$, advance ratio $\mu = 0.148$, hovering tip Mach number $M_{TIP} = 0.645$, and feathering motion. The comparison of pressure distributions predicted by the present method (potential formulation) with the experimental results in [18] is shown in Figs. 1 and 2 which correspond to the blade section at $r/R = 0.97$ for azimuthal angles $\Psi = 180°$ and $\Psi = 270°$. The agreement between the two results is satisfactory, even if the numerical analysis was performed using a prescribed wake geometry (in fact, the wake roll–up is quite irrelevant for advancing rotors; a simple helicoidal wake has been utilized in the present analysis). In Fig. 3 we show the comparison between the measured acoustic signal and the computed one, for an observer placed 2.3m below the rotor disk, at a distance of 3.36m from the rotor hub (micro-

phone 2 in Ref. [20]). The agreement between the two results is satisfactory, even with a numerical analysis performed using a simple helicoidal wake (the wake roll–up is not as relevant for advancing rotors).

Transonic Full–Potential Flows

Next, we present some results concerning transonic full–potential flows. For the sake of completeness, validations for steady two-dimensional flows are presented first, in order to emphasize that the shock–capturing capability is as good as that of other CFD methods, even with a coarser grid. Figure 4 presents the pressure distribution on a circular cylinder at $M_\infty = 0.5$. In this flow configuration a strong shock wave occurs (the local Mach number approaches 3 in the supersonic region). Thus, we are beyond the applicability of the potential model, since the vorticity generated by the discontinuity is not negligible; however, the test case is important to verify the behavior of the present full–potential method in handling strong shocks. The integral solution, obtained using a higher–order numerical scheme, is compared to the solution obtained in [19] using the finite–volume, full–potential code FLO36, based on the scheme of Jameson [20]. The agreement is satisfactory in terms of both shock position and resolution. The same level of accuracy is presented in Fig. 5, where the flow about a NACA 0012 airfoil at $M_\infty = 0.82$ and $\alpha = 0°$ is analyzed. The pressure distribution is compared with both Euler and full–potential finite–volume results (both obtained by Salas [19] using the Jameson scheme [20]). The results (obtained with a C–type grid using 70×20 volume elements) are in good agreement with those obtained by finite volumes, even if a relatively low number of elements is employed. In Fig. 6 the Mach number of the flow around a NACA 0012 airfoil is increased to $M_\infty = 0.84$. In this particular condition a strong shock occurs, and the Euler solution flow cannot be considered potential anymore. Hence, the result of the full–potential integral formulation is compared to a full–potential finite–volume solution [21]. The agreement between the two methodologies is good. The discontinuity obtained with the present approach is confined within one single cell, and the Zierep discontinuity appears to be well captured, despite the relatively coarse grid used for the calculation.

Next, we present some applications for three–dimensional transonic full–potential flows. Consider first a non-lifting 1/7 scale UH-1H hovering rotor with tip Mach number $M_{TIP} = 0.88$. Figure 7 shows the pressure distribution evaluated at $r/R = 0.95$. Comparisons with CFD full–potential and Euler solutions obtained by [22] indicate that there is an acceptable agreement, but the computed shock position is located upwind with respect to that in the reference results. For such a configuration, our full-potential solution obtained with a H-type grid appears to be closer to the CFD Euler one rather than to the CFD full-potential one.
Next, consider a non–lifting rotor in forward flight (blade section $BHT - 540$, hovering Mach number $M_H = 0.665$, advancing ratio $\mu = 0.15$). Figures 8 and 9 show the pressure distribution at section $r/R = 0.92$ for two azimuthal positions ($\Psi = 180°$, and $\Psi = 270°$). The comparison of the numerical results of the present formulation (linear full–potential and nonlinear full–potential) with a numerical solution by a full–potential finite–volume code (Ref. [21], shows a satisfactory agreement. Finally, transonic acoustic results obtained with the present unified aerodynamic/aeroacoustic integral formulation are presented. Again, we consider the 1/7 scale UH-1H non-lifting hovering rotor with tip Mach number $M_{TIP} = 0.85$ (Figs. 10 and 11) and $M_{TIP} = 0.88$ (Figs. 12 and 13). Figures 10 and 12 depict the acoustic pressure (as well as the contribution of body and field sources) computed by the present methodology for an in-plane observer located at a distance $d = 3.09R$ from the rotor. For the same test cases, Figs. 11 and 13 show the numerical results obtained by Ianniello and De Bernardis [23] using a Ffowcs Williams and Hawkings formulation based on CFD aerodynamic data. The agreement of the present results with those in [23] is quite satisfactory, especially in view of the strong dependence upon the tip Mach number (indeed, a 0.03 increase in M_{TIP} determines a doubling of the intensity of the peak of the acoustic signal).

Viscous Transonic Flows

Next, we consider some results obtained by using the present coupled viscous/inviscid technique for the analysis of steady two–dimensional attached high–Reynolds–number transonic flows. The results presented in this Subsection are an

update of those presented in [6], [8], [12], and [24], and are still limited to steady two–dimensional flows; unsteady flows are currently under investigation.

For the present calculations, a C–type grid with adjustable stretch has been utilized for the evaluation of the nonlinear full–potential contributions in the integral equation for the potential, Eq. 6. This yields some improvements of present results with respect to the preliminary results presented in [6] and [24], where an H–type grid is employed. As a test case, we have considered the experimental investigation on the RAE 2822 airfoil, presented in [25]. Specifically, the present analysis refers to two flow conditions (indicated as cases 7 and 9 in [25]) characterized by the presence of an isentropic but relatively strong shock (*i.e.*, Mach number upstream of the shock close to 1.3). Figures 14 and 15 depict, respectively, the numerical results for the pressure coefficient for case 7 ($M_\infty = 0.725$, $Re = 6.5 \times 10^6$, and $\alpha = 2.55°$) and case 9 ($M_\infty = 0.73$, $Re = 6.5 \times 10^6$, and $\alpha = 3.19°$). The comparison of the present numerical results with the experimental ones in [25] shows a satisfactory agreement, both for the prediction of the shock intensity, and for the shock location, which is strongly affected by the effects of viscosity. The agreement between the present calculations and the experiments is satisfactory also for the boundary–layer quantities. This is shown in Figures 16, 17 and 18, that depict, respectively, the friction coefficient, the displacement and the momentum thicknesses, for the case 7 in [25]. Finally, a worthwhile feature of the present boundary–layer/full–potential coupling technique is that the viscosity effects introduced by the coupling renders the full–potential algorithm more stable and its convergence relatively faster; this allows for reducing the artificial viscosity required by the full–potential scheme when the viscous–flow correction is applied.

Concluding Remarks

An overview of some recent developments in the aerodynamic and aeroacoustic analysis of wings and rotors in steady and unsteady compressible flows using the boundary integral formulation for the velocity potential introduced by Morino [1] has been presented. Both subsonic and transonic flows are considered (the transonic analysis is limited to cases in which only weak shocks occur). The effects of viscosity are included by a viscous/inviscid coupling technique, which is valid for attached high–Reynolds number flows. The potential–flow formulation has been applied to obtain the aerodynamic solution for subsonic rotors in forward flight, transonic two–dimensional lifting and non-lifting airfoils, and non-lifting rotors. The coupled boundary–layer/full–potential flow methodology has been applied to steady two–dimensional lifting airfoils in transonic flow. The results presented demonstrate the good level of accuracy of the present methodology as compared to both experimental results and numerical results available in literature. Although additional work appears desirable, the present results are encouraging especially in view of the fact that for this type of applications BEM is well known to be quite inexpensive and highly user friendly. Encouraging results have been obtained for an extension of the formulation to Euler flows (see, Iemma *et al.*, [26]).

Finally, Ref. [27] presents a methodology for obtaining a simple aerodynamic model that facilitates the coupling of the present aerodynamic formulation with flight mechanics and structural dynamics.

Acknowledgements

The results reported in this paper were obtained with partial support from a contract from AGUSTA to the University of Rome III and from the HELISHAPE project, sponsored by the BRITE-EURAM Programme. The contributions of Dott. Ing. Vincenzo Marchese and Dott. Ing. Luigi Luceri are gratefully acknowledged.

References

1. Morino, L., "A General Theory of Unsteady Compressible Potential Aerodynamics," NASA CR 2464, 1974.
2. Morino, L., Gennaretti, M., "Boundary Integral Equations Methods for Aerodynamics." In: Atluri, S.N. (ed.): *Computational nonlinear mechanics in aerospace engineering*, pp. 279–320. AIAA Progress in Aeronautics and Astronautics, 146. Washington, DC, 1992.
3. Morino, L., "Boundary Integral Equations in Aerodynamics," *Appl. Mech. Rev.*, Vol. 46, 1993, pp. 445-466.
4. Gennaretti, M., *Una formulazione integrale di contorno per la trattazione unificata di flussi aeronautici viscosi e potenziali.* Doctoral Dissertation, University of Rome "La Sapienza", Rome, Italy (1993, in Italian).

5. Iemma, U., *Metodi integrali in aerodinamica transonica.* Doctoral Dissertation, University of Rome "La Sapienza", Rome, Italy (1994, in Italian).
6. Salvatore, F., *Forze e momenti su corpi in moto arbitrario in flussi quasi-potenziali e viscosi.* Doctoral Dissertation, University of Rome "La Sapienza", Rome, Italy (1996, in Italian).
7. Gennaretti, M., Iemma, U., Salvatore, F., Morino, L., "A Boundary Element Method for Aerodynamics of Wings and Rotors", Proceedings of the International CEAS/AIAA Forum on Aeroelasticity and Structural Dynamics, Rome, Italy, 1997.
8. Morino, L., Gennaretti, M., Iemma, U., Salvatore, F., "Aerodynamics and Aeroacoustics of Wings and Rotors via BEM – Unsteady, Transonic, and Viscous Effects," accepted for publication in *Computational Mechanics.*
9. Klöppel, V., Kroll, N., Costes, M., Morino, L., Simons, I., Splettstoesser, W., Lowson, M., "The BRITE/EURAM Programme 'HELISHAPE' - A Successful Step to Better Helicopter Aerodynamic and Aeroacoustic Description", Proceedings of the XXIII European Rotorcraft Forum, Dresden, Germany, 1997.
10. Morino, L., Iemma, U., "Boundary Integral Equations and Conservative Dissipation Schemes for Full–Potential Transonic Flows." *Computational Mechanics,* Vol. 13, 1993, pp. 90-99.
11. Lighthill, M.J., "On Displacement Thickness," *J. Fluid Mechanics,* Vol. 4, 1958, pp. 383-392.
12. Morino, L., Salvatore, F., Gennaretti, M., "A Velocity Decomposition for Viscous Flows: Lighthill Equivalent–Source Method Revisited." In: Morino, L., and Wendland, W.L., (eds.): *Boundary Integral Methods for Nonlinear Problems,* pp. 161–166. Kluwer Academic Publishers, Dordrecht, The Netherlands, 1997.
13. Thwaites, B., "Approximate Calculation of the Laminar Boundary Layer," *Aeronaut. Quart.,* Vol. 1, 1949, pp. 245–280.
14. Schlichting, H., *Boundary-Layer Theory,* Mc-Graw Hill: New York, NY, 1979.
15. Michel, R., "Etude de la Transition sur les Profils d'Aile - Establissment d'un Point de Transition et Calcul de la Trainée de Profil en Incompressible," ONERA Report No. 1/1578A, 1952.
16. Green, J.E., Weeks, D.J., and Brooman, W.F., "Prediction of Turbulent Boundary Layers and Wakes in Compressible Flow by a Lag–Entrainment Method," A.R.C.R. & M., no. 3791, 1973.
17. Lemmerman, L.A. and Sonnad, V.R., "Three–Dimensional Viscous–Inviscid Coupling Using Surface Transpiration," *J. Aircraft,* Vol. 16, 1979, pp. 353-358.
18. Splettstoesser, W.R., Junker, B., Schultz, K.J., Wagner, W., Weitemeyer, W., Protopsaltis, A., Fertis, D., "The HELINOISE Aeroacoustic Rotor Test in the DNW - Test Documentation and Representative Results." DLR-Mitt. 93-09, 1993.
19. Salas, M.D., "Recent Developments in Transonic Euler Flow Over a Circular Cylinder." NASA Technical Memorandum no. 83282, Langley Research Center, Hampton, Virginia 1982.
20. Jameson, A., "Transonic Potential Flow Calculation Using Conservation Form." Proceedings of the AIAA 2th Computational Fluid Dynamic Conference, pp. 148-161, 1975.
21. Renzoni, P.G. and Pagano, A., Private Communication, 1997.
22. Prieur, J., Costes, M., Baeder, J.D., "Aerodynamic and Acoustic Calculations of Transonic Nonlifting Hovering Rotors." Proceedings of the International technical specialists meeting on rotorcraft and rotor fluid dynamics, Philadelphia, Penn., 1993.
23. Ianniello, S., De Bernardis, E., Calculation of high speed noise from helicopter rotors using different description of quadrupole source. Proc. AGARD Symposium on Aerodynamics and aeroacoustics of rotorcraft, Berlin, Germany, paper no. 27, 1994.
24. Gennaretti, M., Iemma, U., Salvatore, F., Morino, L., "Irrotational and Rotational Transonic Flows Using a Boundary Integral Equation Method," Proceedings of the XX European Rotorcraft Forum, Amsterdam, The Netherlands, 1994.
25. Cook, P.H., McDonald, M.A., Firmin, M.C.P., "Aerofoil RAE 2822 - Pressure Distribution, and Boundary Layer and Wake Measurements." AGARD AR-138, 1979, paper A6.
26. Iemma, U., Marchese, V., and Morino, L., "Higher Order BEM for Potential and Rotational Inviscid Transonic Aerodynamics" (in preparation).
27. De Troia, R., Gennaretti, Morino, L., "Periodic–Coefficient Finite–State Aerodinamic Modelling for Rotor Dynamics of Helicopter Configurations" *XXII European Rotorcraft Forum,* Dresden, Germany, 1997.

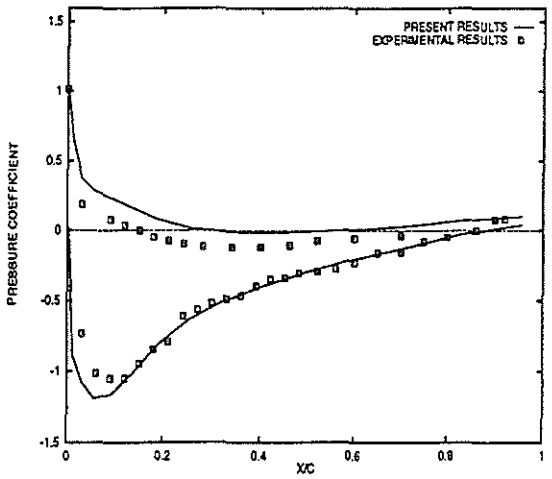

Fig. 1. BO-105 rotor in ascent flight. Pressure coefficient, azimuthal angle $\Psi = 180°$.

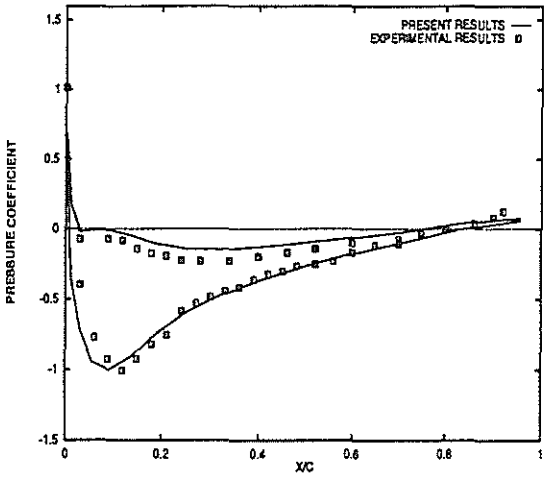

Fig. 2. BO-105 rotor in ascent flight. Pressure coefficient, azimuthal angle $\Psi = 270°$.

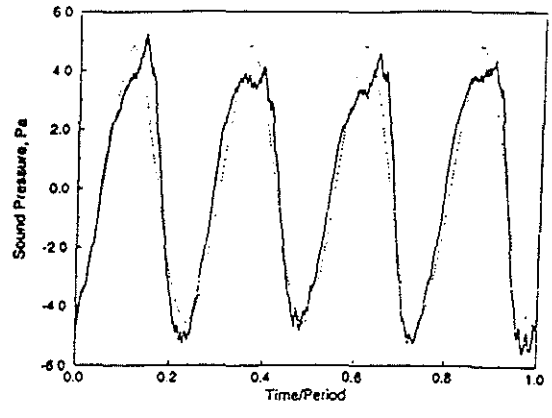

Fig. 3. BO-105 rotor in ascent flight. Acoustic signal.

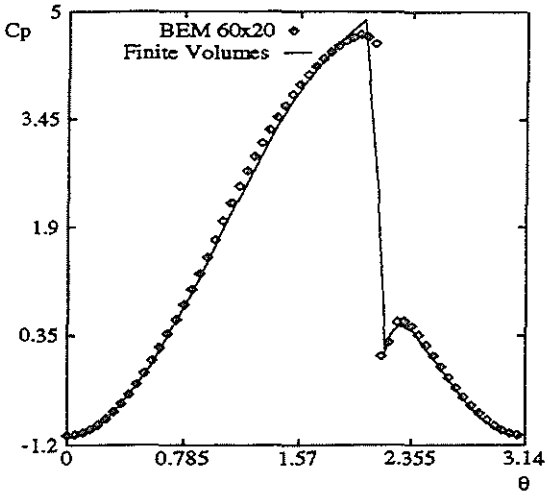

Fig. 4. Pressure coefficient over a circular cylinder with $M_\infty = 0.5$.

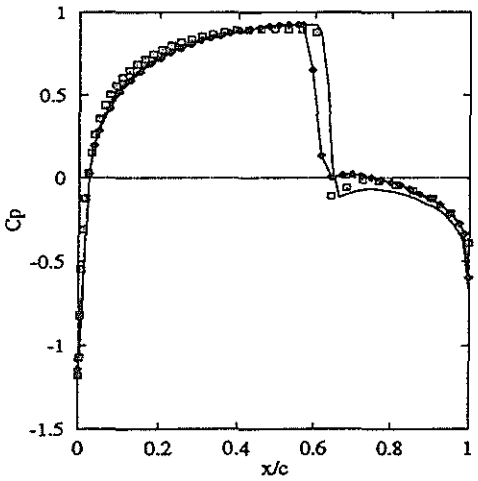

Fig. 5. Pressure coefficient: NACA 0012, $M_\infty = .82$, $\alpha = 0°$. Points: present work; marked line: Ref. [19].

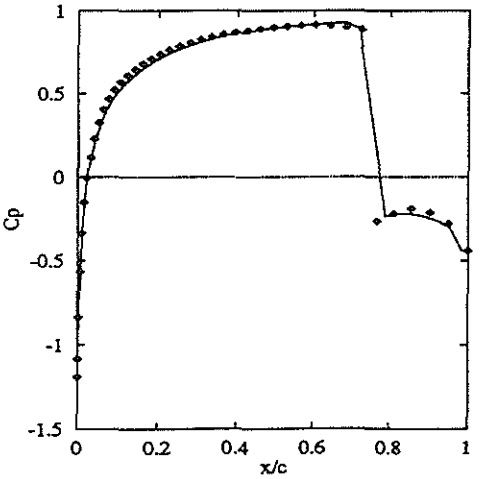

Fig. 6. Pressure coefficient: NACA 0012, $M_\infty = .84$, $\alpha = 0°$. Points: present work; marked line: Ref. [21].

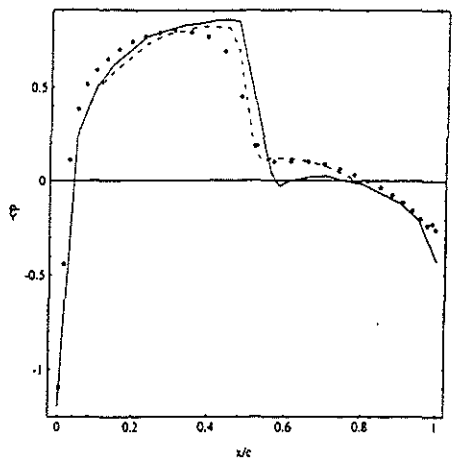

Fig. 7. Non-lifting UH-1H rotor in hover. Chordwise pressure distribution, $r/R = 0.95$.

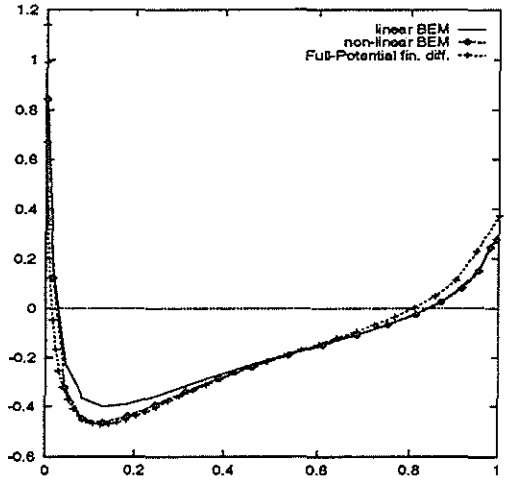

Fig. 8. Non-lifting rotor in forward flight. Chordwise pressure distribution, $r/R = 0.92$, $\Psi = 180°$.

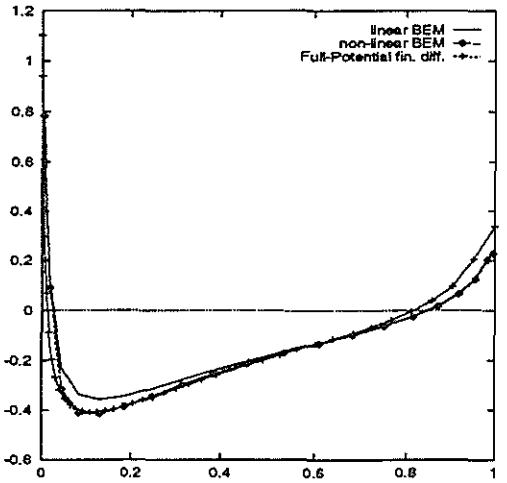

Fig. 9. Non-lifting rotor in forward flight. Chordwise pressure distribution, $r/R = 0.92$, $\Psi = 270°$.

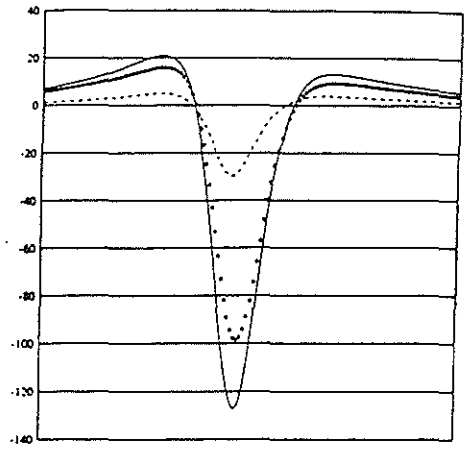

Fig. 10. Non-lifting rotor in forward flight. Acoustic signatures, $M_{TIP} = .85$ (present work).

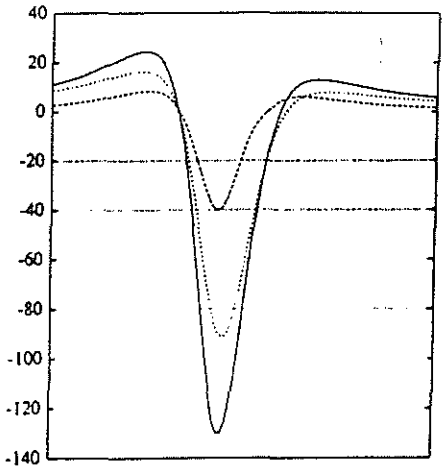

Fig. 11. Non-lifting rotor in forward flight. Acoustic signatures, $M_{TIP} = .85$ (Ref. [23]).

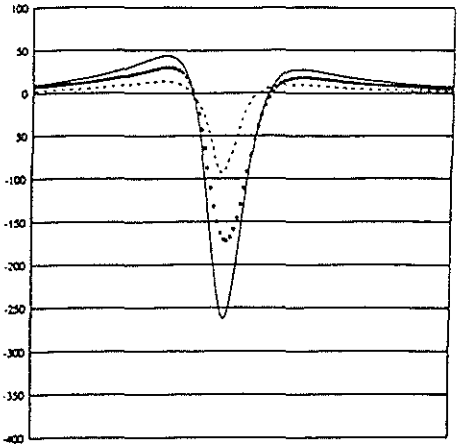

Fig. 12. Non-lifting rotor in forward flight. Acoustic signatures, $M_{TIP} = .88$ (present work).

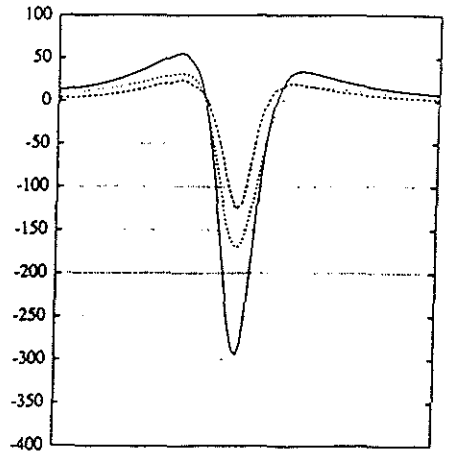

Fig. 13. Non-lifting rotor in forward flight. Acoustic signatures, $M_{TIP} = .88$ (Ref. [23]).

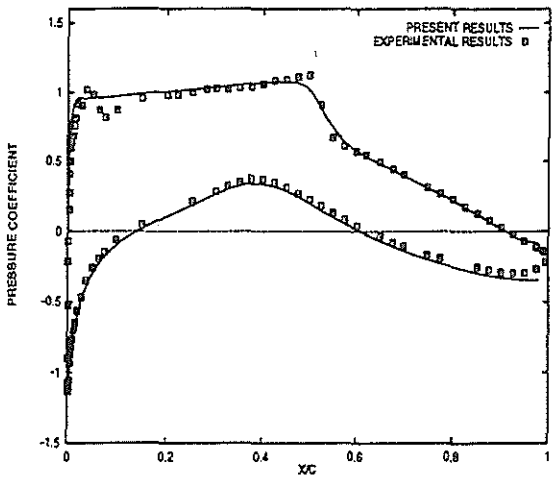

Fig. 14. Pressure coefficient for RAE 2822 airfoil, $M_\infty = 0.725$, $Re = 6.5 \times 10^6$, $\alpha = 2.55°$.

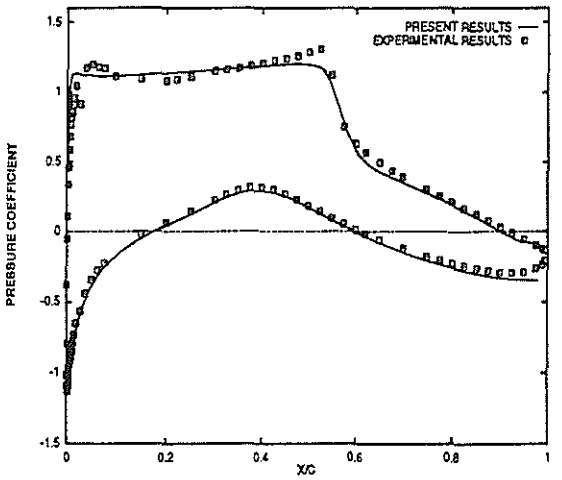

Fig. 15. Pressure coefficient for RAE 2822 airfoil, $M_\infty = 0.73$, $Re = 6.5 \times 10^6$, $\alpha = 3.19°$.

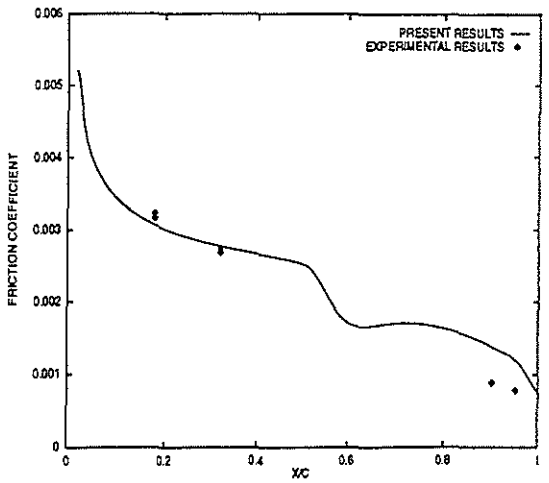

Fig. 16. Friction coefficient for RAE 2822 airfoil, $M_\infty = 0.725$, $Re = 6.5 \times 10^6$, $\alpha = 2.55°$.

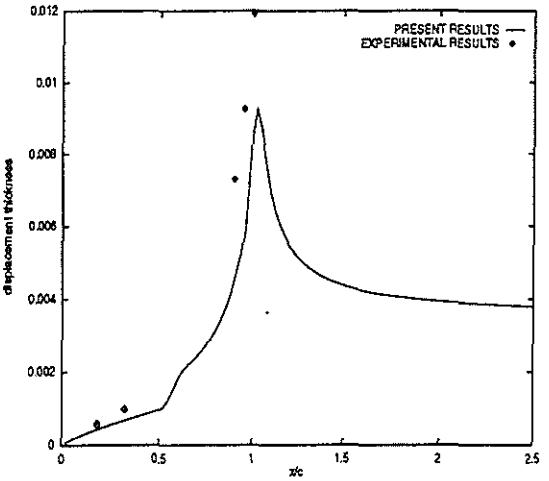

Fig. 17. Displacement thickness for RAE 2822 airfoil, $M_\infty = 0.725$, $Re = 6.5 \times 10^6$, $\alpha = 2.55°$.

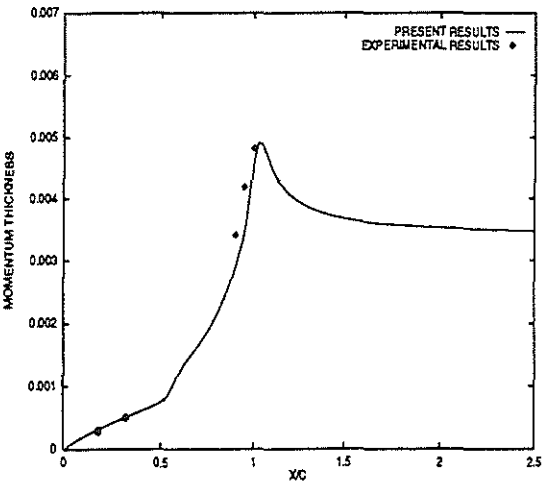

Fig. 18. Momentum thickness for RAE 2822 airfoil, $M_\infty = 0.725$, $Re = 6.5 \times 10^6$, $\alpha = 2.55°$.